Research Square

Preprints are preliminary reports that have not undergone peer review.
They should not be considered conclusive, used to inform clinical practice,
or referenced by the media as validated information.

PdSn Bimetallic Catalysts Prepared by Electroless Deposition for Enhanced n-Butane Dehydrogenation to Butenes

Hemant K Nayak
Indian Institute of Technology Guwahati
Pramod M Gawal
pramodgawal123@gmail.com

Pusan National University, Busan https://orcid.org/0000-0001-8563-5168

Research Article

Keywords: n-Butane dehydrogenation, PdSn bimetallic catalyst, electroless deposition, butenes, metal dispersion, supported catalyst

Posted Date: July 16th, 2026

DOI: https://doi.org/10.21203/rs.3.rs-10362631/v1

License: This work is licensed under a Creative Commons Attribution 4.0 International License.
Read Full License

Additional Declarations: The authors declare no competing interests.

PdSn Bimetallic Catalysts Prepared by Electroless Deposition for Enhanced n-Butane Dehydrogenation to Butenes

Hemant K Nayak[a] and Pramod M Gawal[a,b*]

[a]Department of Chemical Engineering, Indian Institute of Technology Guwahati, Assam-781039, India

[b]Department of Chemistry, Pusan National University, Busan, 46241 South Korea

*Corresponding author: Dr. Pramod M Gawal

Email address: pramodgawal123@gmail.com

Abstract

Efficient n-butane dehydrogenation is a promising route for producing value-added C_4 olefins. In this study, PdSn bimetallic catalysts were synthesized by cyclic electroless deposition on surfactant-modified alumina, zeolite, and silica gel supports. XRD, TEM, EDX, and BET analyses confirmed highly dispersed Pd and Sn species, nanosized metal clusters, successful metal deposition, and support-dependent textural properties. Sn incorporation improved Pd dispersion and enhanced catalytic activity compared with monometallic Pd catalysts. Among the prepared catalysts, PdSn/Sl exhibited the best performance at 550 °C, achieving 68.33% n-butane conversion, 50.65% n-butene yield, and 48.2% iso-butene yield. The superior activity was attributed to Pd–Sn synergistic interaction, improved metal dispersion, and accessible active sites. These results demonstrate that electroless-deposited PdSn catalysts are promising for efficient n-butane dehydrogenation to butenes.

Keywords: n-Butane dehydrogenation; PdSn bimetallic catalyst; electroless deposition; butenes; metal dispersion; supported catalyst

1. Introduction

The increasing demand for light olefins has stimulated extensive research on efficient catalytic routes for alkane dehydrogenation. Butenes are important industrial intermediates used for the production of polymers, synthetic rubber, gasoline additives, petrochemicals, and other value-added chemicals [1–4]. Conventionally, butenes are obtained from naphtha steam cracking and fluid catalytic cracking; however, these processes generally require very high temperatures, show low olefin selectivity, and generate undesired side products and coke [3–5]. Catalytic n-butane dehydrogenation has emerged as an attractive alternative because it directly converts low-cost n-butane into butenes with hydrogen as a valuable co-product and can operate at relatively lower temperatures than steam cracking [3,6].

The direct dehydrogenation of n-butane is highly endothermic and thermodynamically limited, requiring temperatures above 500 °C to achieve appreciable butene yields [4,6,7]. Under such harsh conditions, catalyst deactivation caused by coke deposition, metal sintering, cracking, hydrogenolysis, and isomerization becomes a major challenge [3,4,6]. High reaction temperature can also promote C–C bond cleavage, resulting in the formation of lighter hydrocarbons and reduced selectivity toward the desired C_4 olefins [3,5]. Oxidative dehydrogenation using O_2 or CO_2 has also been explored to overcome thermodynamic limitations; however, issues such as deep oxidation, competing dry reforming, and product over-oxidation can reduce olefin selectivity [8,9]. Therefore, the development of catalysts with high activity, selectivity, and stability remains essential for efficient n-butane dehydrogenation.

Noble metal-based catalysts, particularly Pt- and Pd-supported catalysts, have been widely investigated for light alkane dehydrogenation because of their strong ability to activate C–H bonds [3,10,11]. Pt-based catalysts are highly active, but monometallic Pt catalysts often suffer from poor olefin selectivity and rapid deactivation due to coke formation and secondary reactions [4,6]. Pd-

based catalysts are also attractive because palladium is comparatively less expensive than platinum and possesses good hydrogenation–dehydrogenation activity [3,12]. However, monometallic Pd catalysts can show similar limitations, including strong hydrocarbon adsorption, cracking, coke formation, and limited stability during dehydrogenation reactions [3,10,13].

The incorporation of a second metal into noble metal catalysts is an effective strategy to improve catalytic performance. Bimetallic catalyst design is widely recognized as a powerful approach for tuning activity, selectivity, and stability through metal–metal synergy, electronic modification, ensemble effects, and improved surface structure [14–16]. Promoters such as Sn, Ga, Cu, In, Ag, and Pb can modify the electronic and geometric properties of noble-metal active sites, reduce the ensemble size, suppress C–C bond cleavage, and improve olefin selectivity [9–11,13,17]. Cu addition to Pd/Al_2O_3 was reported to increase n-butane conversion and C_4 selectivity through improved metal dispersion and alloy formation [11]. Similarly, Ni-, Cu-, and Ag-promoted Pd/Al_2O_3 catalysts prepared by electroless co-deposition showed improved butane conversion, butene yield, and catalyst stability compared with monometallic Pd catalysts [13].

Among different promoters, Sn has attracted considerable attention as a promoter for dehydrogenation catalysts because it can form alloy or intermetallic phases with noble metals, isolate highly active metal ensembles, weaken excessive alkene adsorption, and reduce coke formation [4,6,17]. Previous studies on Pt–Sn catalysts have shown that Sn addition can modify the geometric structure of Pt particles, decrease hydrogenolysis and coke formation, and improve selectivity toward olefins during n-butane dehydrogenation [4,6]. Strong metal–support interaction in $Pt–Sn/SiO_2$ catalysts has also been shown to influence metal dispersion, Sn-enriched alloy formation, and catalytic behavior in lower alkane dehydrogenation [17].

Although Pt–Sn catalysts have been extensively studied, Pd-based bimetallic catalysts for n-butane dehydrogenation remain relatively less explored [3,10]. Earlier reports showed that the addition of Sn to Pd-based catalysts improved dehydrogenation selectivity in propane

dehydrogenation, while Ga-modified Pd/Al_2O_3 catalysts exhibited higher butene selectivity than monometallic Pd catalysts in n-butane dehydrogenation [3,12]. Pd-based intermetallic compounds have also shown enhanced dehydrogenation selectivity because the second metal can regulate the catalytic environment around Pd and suppress undesired combustion or secondary reactions [9]. These findings suggest that PdSn-based bimetallic catalysts can be promising alternatives to conventional Pt-based systems.

Apart from catalyst composition, the synthesis method strongly influences metal dispersion, particle size, alloy formation, and metal–support interaction. Conventional impregnation methods often lead to non-uniform metal distribution, larger particles, and weak metal–support interactions. In contrast, modified electroless deposition provides a controlled route for depositing metal species directly on the support surface without external electrical energy. This method can enhance metal dispersion, promote stronger metal–support interaction, and improve catalytic activity and stability [3,13]. Saxena and De reported that alumina-supported Pd–Pt bimetallic catalysts prepared by modified electroless deposition showed superior butane dehydrogenation performance compared with monometallic catalysts, mainly due to synergistic metal interaction, stronger metal–support interaction, lower acidity, and reduced secondary reactions [3]. Similarly, Ni-, Cu-, and Ag-promoted Pd/Al_2O_3 catalysts prepared by electroless co-deposition showed improved butane conversion, butene yield, and stability, confirming that controlled co-deposition can promote strong Pd–promoter interaction, alloy formation, and better catalyst performance [13].

The support also plays a critical role in determining catalyst performance by influencing metal dispersion, acidity, pore structure, and reactant/product diffusion. Supports such as alumina, silica, zeolite, and mesoporous oxides have been widely used in alkane dehydrogenation reactions [3,5,7,18]. Mesoporous supports can facilitate mass transfer and stabilize small metal particles, while zeolitic supports provide high surface area and shape-selective properties [7,18]. However, excessive acidity may promote cracking and coke formation, thereby lowering butene selectivity [5,18].

Therefore, tuning the support properties together with the Pd–Sn interaction is important for optimizing catalytic performance [18].

In the present study, PdSn-based bimetallic catalysts were synthesized through a modified electroless deposition method using different supports, including alumina, surfactant-modified alumina, silica gel, and zeolite. The catalysts were characterized using XRD, BET, TEM, and EDX to understand their structural, textural, morphological, and compositional properties. Their catalytic performance was evaluated for n-butane dehydrogenation at 550 °C. The study aims to clarify the effect of Sn incorporation and support nature on Pd dispersion, Pd–Sn interaction, butane conversion, and butene selectivity. The prepared PdSn catalysts showed improved performance compared with monometallic Pd catalysts, with PdSn/Sl giving the highest butane conversion and PdSn/Z showing the highest n-butene selectivity, confirming the importance of Pd–Sn synergy and support effects in butane dehydrogenation.

2. Experimental section

2.1 Materials

Palladium chloride ($PdCl_2$) (99.9%), silica gel, zeolite, and Tin (II) chloride ($SnCl_2$) dehydrate (98%), zeolite (Z) (98 %) and alumina gel (SI) (99%) were purchased from Sigma-Aldrich, USA. Aluminum nitrate (99%) and hydrochloric acid (HCl) (37%), hydrazine was obtained from Merck, India. Ammonia solution was purchased from Thermo Fisher Scientific, India. Sodium dodecyl sulfate (SDS) (99%) was purchased from SRL, India. All experiments were performed utilizing distilled water (DW) obtained from a water purifier (Millipore, Germany).

2.2 Synthesis of catalyst

The alumina (Al) support was synthesized by a precipitation method using aluminum nitrate as the precursor, as shown in **Fig. S1**. In a typical procedure, a calculated amount of $Al(NO_3)_3$ was dissolved in distilled water to obtain a clear aluminum nitrate solution. The solution was stirred for 15 min at room temperature to ensure complete dissolution and homogeneity. Subsequently, 30% ammonia solution was added dropwise under continuous stirring to hydrolyze the aluminum precursor, while maintaining the pH at approximately 10.5. The resulting mixture was further stirred for 60 min at room temperature to complete the precipitation of aluminum hydroxide. The obtained aluminum hydroxide precipitate was then aged at 75 °C for 6 h to improve the structural development of the precursor. After aging, the precipitate was collected by filtration and washed thoroughly with DW to remove residual ions and impurities. The washed sample was dried at 100 °C for 24 h in a hot-air oven. Finally, the dried precursor was calcined at 550 °C for 6 h to obtain alumina (Al_2O_3). For the preparation of surfactant-modified alumina (AlS), sodium dodecyl sulfate (SDS) solution was introduced into the aluminum nitrate solution before the precipitation step. The remaining synthesis procedure, including ammonia hydrolysis, aging, washing, drying, and calcination, was kept the same as that used for alumina preparation.

The supported palladium catalysts were synthesized using an electroless deposition method, as shown in **Fig. S2**. In this method, hydrazine solution was used as the reducing agent, while $PdCl_2$ was used as the metal precursor. The $PdCl_2$ solution was prepared in distilled water, and the pH was adjusted to approximately 2 using 37% HCl. In a typical synthesis, the support was placed in a Buchner funnel under vacuum filtration. First, 20 mL of hydrazine solution was passed through the support and allowed to remain in contact for 10 min. Subsequently, 20 mL of Pd precursor solution was slowly poured through the hydrazine-treated support and maintained for another 10 min to promote Pd deposition. These two steps completed the first deposition cycle. The filtrate collected after the first cycle, containing residual hydrazine and Pd precursor, was reused for the second cycle to enhance metal utilization and improve Pd deposition. After completion of the second cycle, fresh

hydrazine and Pd precursor solutions were introduced for the third cycle, followed by reuse of the corresponding filtrate in the fourth cycle. Thus, the catalyst preparation involved four deposition cycles, where fresh solutions were used in the first and third cycles, while filtrates were reused in the second and fourth cycles. After completion of the cyclic deposition process, the resulting wet catalyst was collected, filtered, and dried in an oven at 110 °C for 12 h. The catalysts prepared using alumina and surfactant-modified alumina supports were denoted as Pd/Al and Pd/AlS, respectively.

The PdSn/AlS bimetallic catalyst was prepared using a cyclic electroless deposition method, as illustrated in **Fig. 1**. In the first cycle, modified alumina (AlS) was treated with 20 mL of acidic $SnCl_2$ solution, with the pH adjusted to approximately 2.7 using HCl. During this step, Sn^{2+} ions were adsorbed onto the AlS surface, forming an AlS–$SnCl_2$ intermediate. Subsequently, 20 mL of Pd precursor solution was slowly introduced, where the surface-adsorbed Sn^{2+} species acted as both a reducing agent and a secondary metal source, facilitating the reduction of Pd^{2+} to metallic Pd and forming Pd/AlS. The filtrate collected after the first deposition step was reused in the second cycle to improve metal utilization and deposition efficiency. In the third cycle, a fresh $SnCl_2$ solution was again added to the Pd/AlS catalyst to generate Pd/AlS–$SnCl_2$, followed by the addition of Pd precursor solution in the fourth cycle using the corresponding filtrate. Through these repeated $SnCl_2$ activation and Pd deposition steps, Pd and Sn species were deposited on the AlS support, leading to the formation of the PdSn/AlS bimetallic catalyst. Thus, the synthesis involved four cyclic deposition steps, in which fresh solutions were used in the first and third cycles, while the collected filtrates were reused in the second and fourth cycles. Finally, the obtained PdSn/AlS catalyst was filtered, washed thoroughly with distilled water, and dried before further characterization and catalytic testing. The same procedure was followed for the preparation of PdSn/Sl and PdSn/Z catalysts, with only the support changed from AlS to silica gel (Sl) and zeolite (Z), respectively.

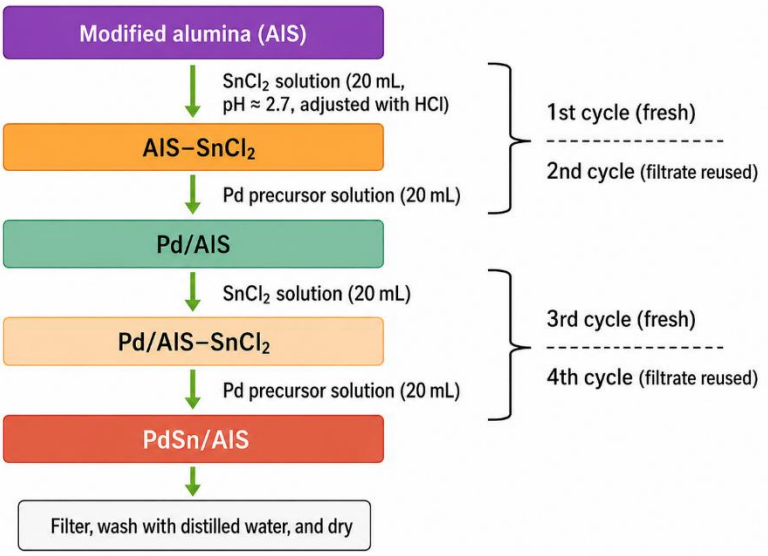


Figure 1. Schematic illustration of the cyclic electroless deposition method used for the preparation of PdSn/AlS bimetallic catalyst.

2.3. Characterizations

The crystalline structure of the synthesized catalyst was analyzed using a powder X-ray diffractometer (XRD, Smart lab, Rigaku, Japan) with Cu Kα radiation, scanning in the 2θ range of 10 to 80° at a scan rate of 20° min^{-1}. The surface area of the catalysts was determined by studying the N_2 adsorption-desorption isotherm using a BET analyzer (Micromeritics, Tristar-II 3020, USA). Fourier transform infrared spectroscopy (FTIR, Affinity 1, Shimadzu, Japan) was used to analyze the functional groups. The morphological attributes of the catalyst particles were investigated using a field emission scanning electron microscope (FESEM, Sigma 300, Zeiss, Germany) and a field emission transmission electron microscope (FETEM, JEM2100F, JEOL, Japan) to determine particle sizes and morphology. The elemental compositions were determined using a field emission scanning electron microscope (FESEM) with an element EDS detector (Sigma 300, Zeiss, Germany).

2.4. Dehydrogenation activity measurements

The catalytic performance of the synthesized catalysts for n-butane dehydrogenation was evaluated in a fixed-bed continuous downflow reactor, as illustrated in **Fig. 2**. The reaction was

carried out at 550 °C under atmospheric pressure. In a typical experiment, 0.25 g of catalyst was physically mixed with 1 g of quartz powder and loaded at the center of the reactor. A thermocouple was placed in contact with the catalyst bed to accurately monitor and control the reaction temperature. The feed gas mixture consisted of n-butane, H_2, and N_2 in a molar ratio of 1:3:6. The individual gas flow rates were adjusted to 10 mL/min for n-butane, 30 mL/min for H_2, and 60 mL/min for N_2, giving a total flow rate of 100 mL/min. The gas flow was regulated using rotameters and a mass flow controller before entering the reactor. The reactor temperature was maintained using a temperature controller.

The outlet gas stream from the reactor was analyzed using gas chromatography (450-GC, Bruker, USA) equipped with a thermal conductivity detector (TCD) and a 60/80 Carboxen 1000 column (15 ft × 1/8 in × 2.1 mm). The GC oven temperature was initially maintained at 40 °C for 5 min and then increased to 200 °C at a heating rate of 20 °C/min. The injector and detector temperatures were maintained at 100 and 200 °C, respectively. Nitrogen was used as the carrier gas at a flow rate of 30 mL/min. The chromatographic data were recorded and processed using a computer system.

The main dehydrogenation reaction of n-butane can be represented as:

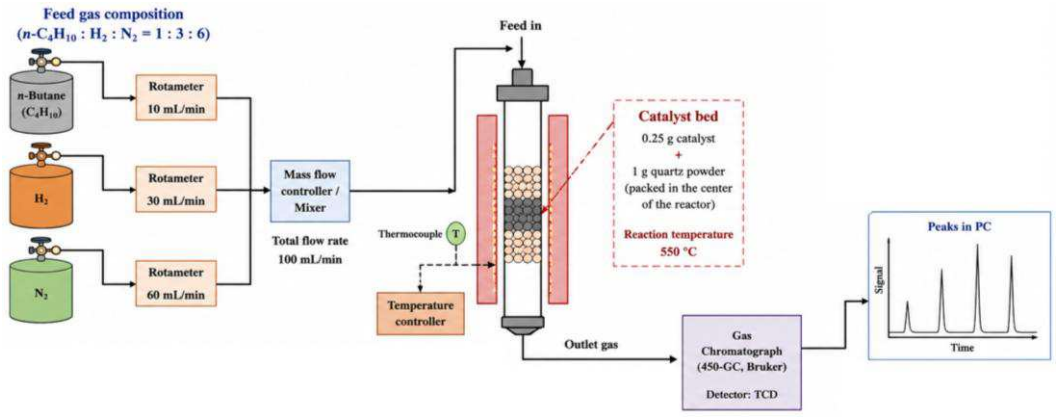
$$C_4H_{10} \rightarrow C_4H_8 + H_2 \quad (1)$$

The catalytic performance was evaluated in terms of n-butane conversion, product selectivity, and yield using the following equations:

$$Butane\ conversion\ (\%) = \frac{Mole\ of\ butane\ in - mole\ of\ butane\ out}{mole\ of\ buatne\ in} \times 100 \quad (2)$$

$$Yied\ \ (\%) = \frac{Mole\ of\ n-butene\ or\ iso-butene\ formrd}{mole\ of\ butane\ supplied} \times 100 \quad (3)$$

$$Selectivity\ of\ product\ \ P\ \ (\%) = \frac{Mole\ of\ \ product\ P\ formed}{Total\ moles\ of\ product\ formed} \times 100 \quad (4)$$



226

227 **Figure 2.** Schematic diagram of the fixed-bed continuous downflow reactor system used for n-butane
228 dehydrogenation.

229

230 # 3. Results and discussion

231 ## 3.1 Characterization of the catalyst

232 ***XRD Analysis:*** X-ray diffraction analysis was performed to examine the crystalline structure
233 of the supports, monometallic Pd catalysts, and PdSn bimetallic catalysts. As shown in **Fig. 3a**, Al
234 and AlS exhibited broad and weak diffraction peaks, indicating their predominantly amorphous or
235 poorly crystalline nature. The weak reflections at approximately 38.6°, 45.7°, and 66.8° can be
236 assigned to γ-Al_2O_3 [3]. The AlS support showed similar diffraction features, suggesting that
237 surfactant modification did not significantly change the alumina structure. Silica gel showed a broad
238 diffraction band near 25°, confirming its amorphous nature, whereas zeolite exhibited sharp and
239 intense peaks, indicating its crystalline framework. The XRD patterns of Pd/Al and Pd/AlS are shown
240 in **Fig. 3b**. Both catalysts retained the characteristic features of their alumina-based supports. The
241 expected metallic Pd reflections at around 40.1°, 46.1°, and 68.1° were not clearly observed,
242 probably due to low Pd loading, small crystallite size, high Pd dispersion, and overlap with γ-Al_2O_3
243 peaks. Similar absence of distinct noble-metal peaks has been reported for highly dispersed supported
244 bimetallic catalysts prepared by electroless deposition [13].

The XRD patterns of PdSn-based bimetallic catalysts are shown in **Fig. 3c**. PdSn/AlS and PdSn/Sl exhibited broad diffraction features corresponding to alumina- and silica-based supports, while PdSn/Z retained the crystalline peaks of the zeolite support. No distinct diffraction peaks corresponding to metallic Pd, Sn, SnO_2, or Pd–Sn alloy phases were detected, suggesting that Pd and Sn species were highly dispersed or existed as very small crystallites below the XRD detection limit. Thus, Pd and Sn deposition did not significantly alter the bulk structure of the supports, confirming the suitability of the electroless deposition method for preparing well-dispersed supported PdSn catalysts. Sn modification has also been reported to tune noble-metal sites, suppress C–C bond cleavage, reduce coke formation, and improve olefin selectivity during alkane dehydrogenation [4].

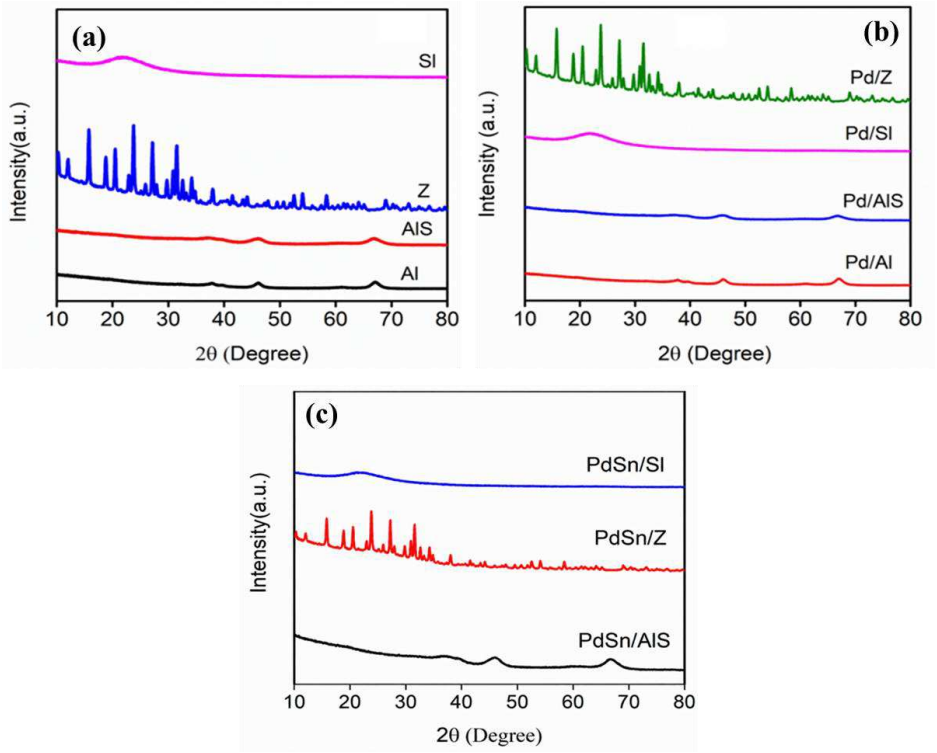
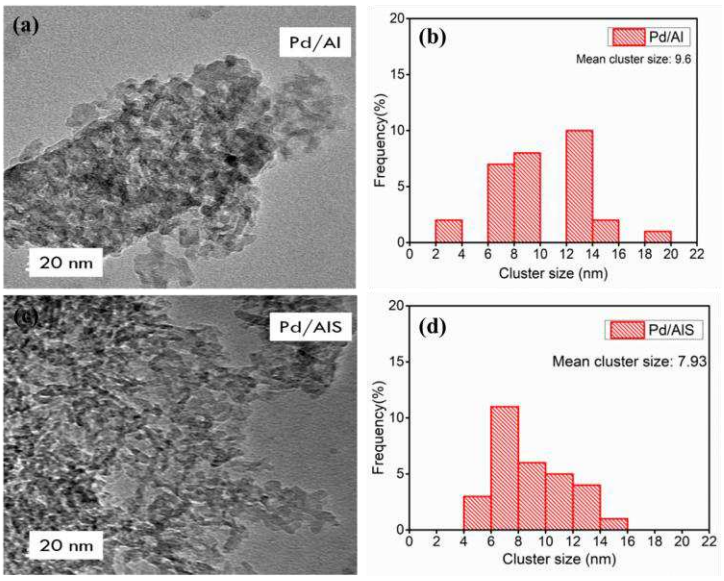


Figure 3. XRD patterns of (a) different supports, including Al, AlS, Z, and Sl, (b) monometallic Pd catalysts supported on Al, AlS, Z, and Sl, and (c) PdSn-based bimetallic catalysts supported on AlS, Z, and Sl.

***TEM analysis*:** TEM analysis was performed to evaluate the morphology, dispersion, and metal-cluster size of the synthesized catalysts. As shown in **Fig. 4**, the monometallic Pd/Al and

Pd/AlS catalysts exhibited average metal-cluster sizes of 9.6 and 7.93 nm, respectively. The smaller cluster size of Pd/AlS indicates that surfactant modification improved Pd dispersion, likely due to enhanced metal–support interaction. In contrast, Pd/Al showed relatively larger and more agglomerated particles, which may reduce the number of accessible active sites. The TEM images of PdSn-based bimetallic catalysts are shown in **Fig. 5**. The average cluster sizes were 7.16 nm for PdSn/AlS, 8.36 nm for PdSn/Z, and 8.9 nm for PdSn/Sl. The smaller particle size of PdSn/AlS compared with monometallic Pd catalysts suggests that Sn incorporation suppressed Pd agglomeration and promoted better metal dispersion. This behavior is consistent with earlier reports showing that second-metal addition can improve metal dispersion, reduce active metal ensemble size, and enhance catalytic performance in butane dehydrogenation catalysts [3,13].

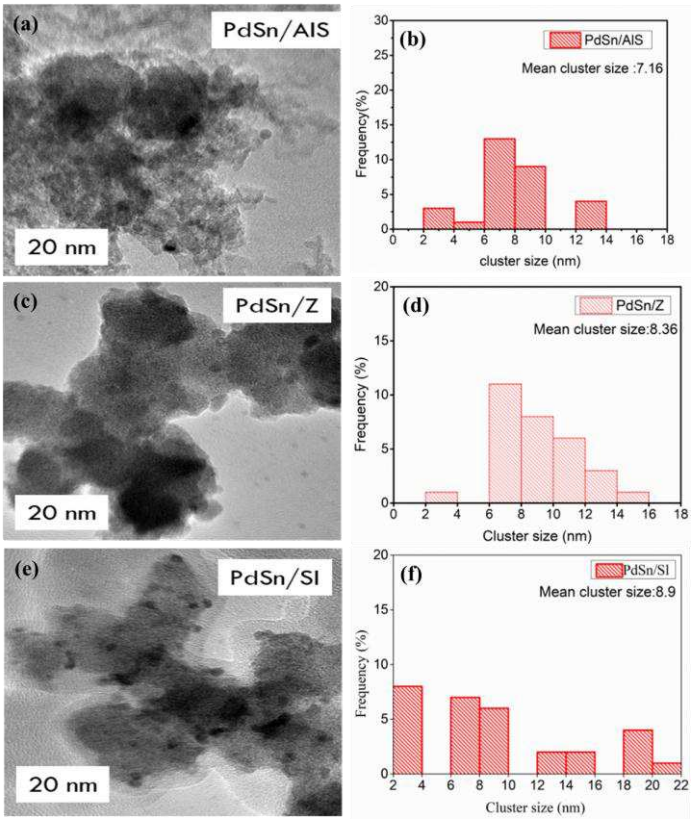
Among the bimetallic catalysts, PdSn/AlS showed the smallest cluster size, indicating a stronger interaction between PdSn species and the surfactant-modified alumina support. The slightly larger clusters in PdSn/Z and PdSn/Sl suggest that support properties such as pore structure, surface area, and acidity influence metal nucleation and growth. The TEM results confirm that cyclic electroless deposition successfully produced nanosized PdSn clusters, and Sn incorporation improved metal dispersion, which is beneficial for enhancing n-butane dehydrogenation activity. Sn-modified noble-metal catalysts have also been reported to suppress hydrogenolysis, cracking, and coke formation by modifying the geometric and electronic structure of active metal sites [4].



278

279 **Figure 4.** TEM images and corresponding particle-size distribution histograms of monometallic Pd

280 catalysts: (a,b) Pd/Al and (c,d) Pd/AlS.



281

282 **Figure 5.** TEM images and corresponding particle-size distribution histograms of PdSn-based

283 bimetallic catalysts: (a,b) PdSn/AlS, (c,d) PdSn/Z, and (e,f) PdSn/Sl.

***EDX analysis*:** EDX analysis was carried out to confirm the elemental composition and successful deposition of Pd and Sn on different supports. As summarized in **Table 1**, Pd was detected in both monometallic catalysts, with loadings of 1.6 wt% for Pd/Al and 1.8 wt% for Pd/AlS, confirming successful Pd deposition by the electroless method. The slightly higher Pd loading in Pd/AlS suggests that surfactant-modified alumina provided more favorable surface sites for metal deposition. For the bimetallic catalysts, both Pd and Sn were detected, confirming the formation of PdSn-based systems. The Pd loading varied from 1.6 to 3.5 wt%, while Sn loading ranged from 4.4 to 9.4 wt%. PdSn/Sl showed the highest Pd loading of 3.5 wt%, whereas PdSn/Z exhibited the highest Sn loading of 9.4 wt%. The presence of Si and Na in PdSn/Z originated from the zeolite framework, while Al and O were associated with the alumina-based supports. These results indicate that metal deposition was strongly influenced by support composition, surface chemistry, and porosity.

The successful incorporation of Sn is important because Sn can modify the electronic and geometric environment of noble-metal sites, promote metal–metal interaction, and suppress undesired cracking, hydrogenolysis, and coke formation during alkane dehydrogenation [4,6]. Similar observations have been reported for promoted Pd/Al_2O_3 catalysts prepared by electroless co-deposition, where EDX confirmed the presence of Pd and promoter metals and demonstrated support-dependent metal distribution [13]. Overall, EDX results confirm the successful preparation of monometallic Pd and bimetallic PdSn catalysts with support-dependent metal loading.

Table 1. EDX elemental composition of monometallic Pd and PdSn-based bimetallic catalysts prepared on different supports.

Sample ID	**Elements analysis (wt%)**					
	Al	**O**	**Pd**	**Sn**	**Si**	**Na**
Pd/Al	49.3	31.4	1.6	0.0	0.0	0.0
Pd/AlS	46.7	38.8	1.8	0.1	0.0	0.0

PdSn/AlS	37.6	55.9	2.1	4.4	0	0
PdSn/Sl	48.1	41.3	3.5	7.1	0	0
PdSn/Z	16.9	53.8	1.6	9.4	17.3	0.8

***BET analysis*:** properties of the supports and catalysts. The isotherms and pore-size distributions are shown in **Fig. 6**, and the corresponding BET surface area, pore volume, and average pore diameter are summarized in **Table 2**. Al and AlS exhibited type IV isotherms with hysteresis loops, confirming their mesoporous nature. The BET surface area increased from 218 m^2/g for Al to 299 m^2/g for AlS, while the pore volume increased from 0.3 to 0.7 cm^3/g, indicating that SDS-assisted modification improved the mesoporosity of alumina. The textural properties varied significantly with support type. Sl and Z showed higher surface areas of 740 and 697 m^2/g, respectively. However, Z exhibited mainly microporous characteristics with a small average pore diameter of 1.1 nm, whereas Sl showed mesoporous features with an average pore diameter of 5.7 nm. After Pd deposition, Pd/Al and Pd/AlS retained mesoporous structures with surface areas of 219 and 307 m^2/g, respectively. Such mesoporous structures are beneficial for reactant and product diffusion during n-butane dehydrogenation [19–21].

For the PdSn-based catalysts, the BET surface areas of PdSn/AlS, PdSn/Z, and PdSn/Sl were 334.4, 347.3, and 222.4 m^2/g, respectively. Although PdSn/Z showed the highest surface area, its pore volume decreased sharply to 0.013 cm^3/g, suggesting partial blockage of zeolite micropores after Pd and Sn deposition. In contrast, PdSn/AlS retained a high pore volume of 0.8 cm^3/g and an average pore diameter of 9.1 nm, indicating an open mesoporous structure. The decrease in pore volume after metal deposition is consistent with previous reports on supported bimetallic catalysts, where metal incorporation partially blocks pore channels [3,13]. Overall, BET results confirm that the catalysts possess support-dependent textural properties. The mesoporous structure of PdSn/AlS and PdSn/Sl can facilitate mass transfer, whereas the very low pore volume of PdSn/Z may restrict

pore accessibility. Mesoporous supported PtSn catalysts have also been reported to stabilize metal particles and improve catalytic performance in n-butane dehydrogenation [4].

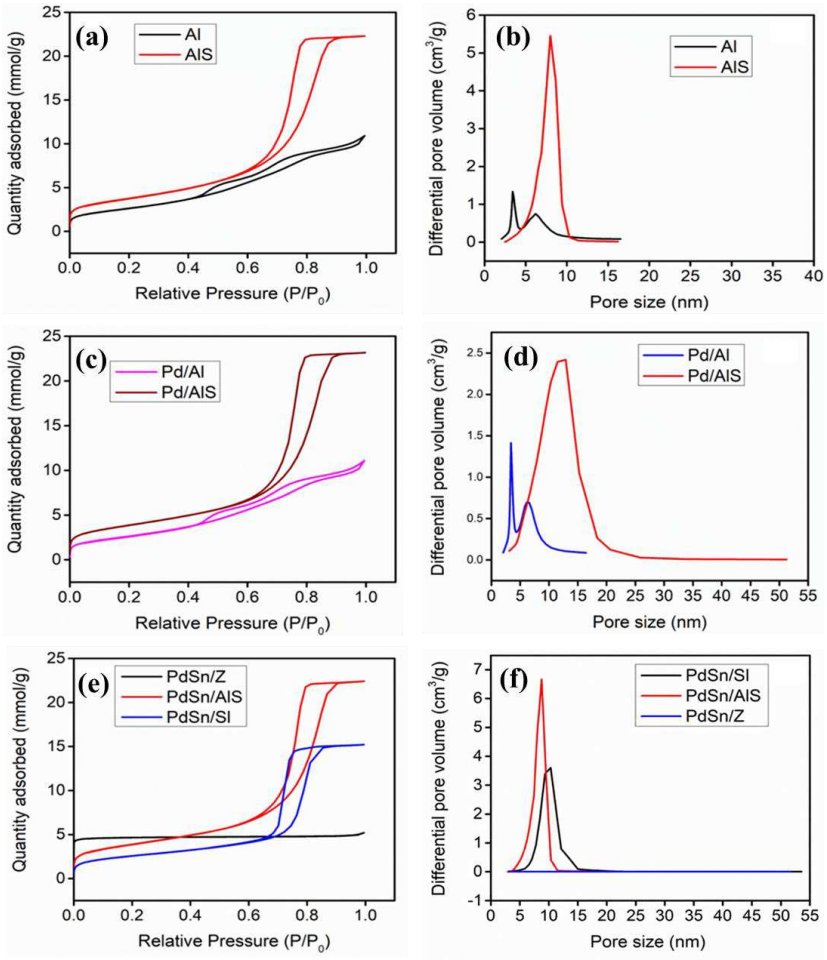


Figure 4. Nitrogen adsorption–desorption isotherms and pore-size distribution curves of different supports and catalysts: (a,b) Al and AlS supports, (c,d) monometallic Pd/Al and Pd/AlS catalysts, and (e,f) PdSn-based bimetallic catalysts supported on AlS, Z, and Sl.

Table 2. Textural properties of the synthesized supports, monometallic Pd catalysts, and PdSn-based bimetallic catalysts.

Sample ID	BET surface area (m^2/g)	Pore volume (cm^3/g)	Average pore diameter (nm)
Al	218	0.3	5.6
AlS	299	0.7	8.7

Sl	740	0.6	5.7
Z	697	0.4	1.1
Pd/Al	219	0.3	5.9
Pd/AlS	307	0.8	9.1
PdSn/AlS	334.4	0.8	9.1
PdSn/Z	347.3	0.013	5.4
PdSn/Sl	222.4	0.5	8.9

Al:alumina;AlS:surfactantmodifiedalumina;Sl:silicagel;Z:zeoli

3.2. Dehydrogenation activity tests

The catalytic performance of monometallic Pd and PdSn-based bimetallic catalysts was evaluated for n-butane dehydrogenation at 550 °C, and the results are shown in **Fig. 7** and **Table 3**. The conversion strongly depended on catalyst composition and support. Monometallic Pd/Al and Pd/AlS showed low conversions of 6.65% and 7.65%, respectively, whereas PdSn-based catalysts exhibited much higher activity. The conversion followed the order: PdSn/Sl (68.33%) > PdSn/Z (64.35%) > PdSn/AlS (56.85%) > Pd/AlS (7.65%) > Pd/Al (6.65%) (**Fig. 7a**). The improved activity of PdSn catalysts can be attributed to Pd–Sn synergistic interaction, enhanced metal dispersion, and modification of Pd active sites, as reported for other bimetallic dehydrogenation catalysts [3,13]. The n-butene yield also increased after Sn incorporation. PdSn/Sl showed the highest n-butene yield of 50.65%, followed by PdSn/Z (45.55%) and PdSn/AlS (39.3%), while Pd/Al and Pd/AlS showed lower yields of 17.25% and 26.7%, respectively (**Fig. 7b**). Similarly, PdSn/Sl gave the highest iso-butene yield of 48.2% (**Fig. 7c**). The improved olefin yield over PdSn catalysts may be due to electronic and geometric modification of Pd sites by Sn, which can suppress hydrogenolysis, cracking, and coke formation [4,6].

The selectivity results showed that Pd/Al had the highest n-butene selectivity of 63.96%, while PdSn catalysts showed slightly lower n-butene selectivity but much higher conversion and

overall olefin yield. Among the bimetallic catalysts, n-butene selectivity followed the order PdSn/AlS (53.35%) > PdSn/Z (52.56%) > PdSn/Sl (51.81%) (**Fig. 7d**). The slight decrease in n-butene selectivity at higher conversion may be related to secondary isomerization reactions and support acidity, as also observed for Pt–Sn/ZSM-5 catalysts [18]. Overall, PdSn/Sl exhibited the best catalytic performance, with the highest n-butane conversion, n-butene yield, and iso-butene yield. This confirms that Sn incorporation and support selection play important roles in improving Pd-based catalysts for n-butane dehydrogenation. Similar promotional effects of second metals have been reported for Pd–Cu, Pd–Ag, Pd–Ga, and Pt–Sn systems [10,11,13]. The present catalytic results were also compared with reported literature on Pd-, Pt-, and bimetallic catalysts for n-butane dehydrogenation (**Table S1**), indicating that PdSn/Sl exhibits competitive activity and improved butene yield under the present reaction conditions.

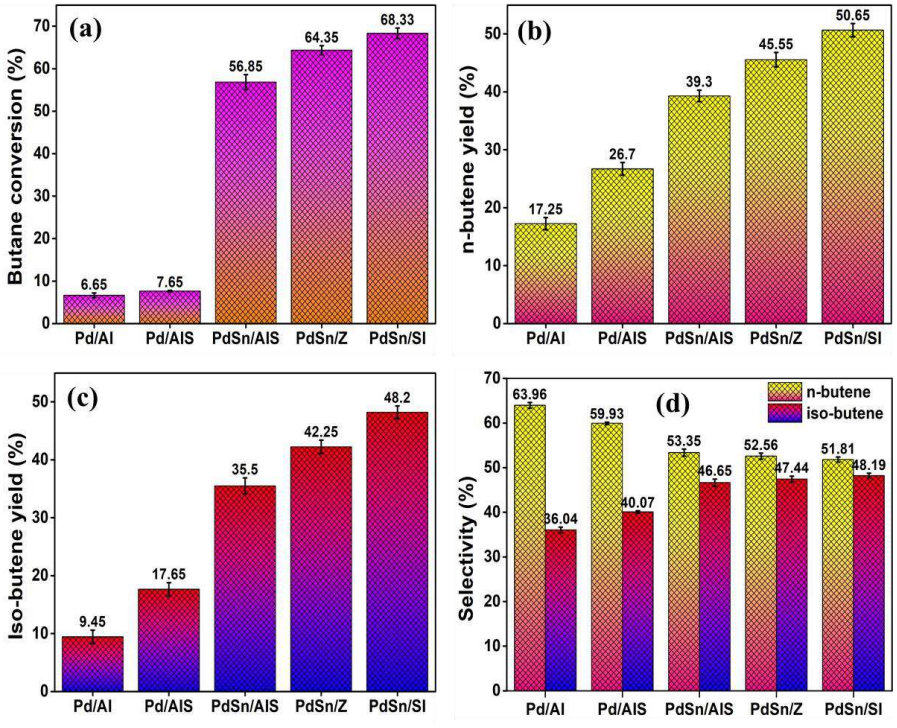


Figure 7. Catalytic performance of monometallic Pd and PdSn-based bimetallic catalysts for n-butane dehydrogenation at 550 °C: (a) n-butane conversion, (b) n-butene yield, (c) iso-butene yield, and (d) n-butene and iso-butene selectivity.

Table 3. Catalytic performance of monometallic Pd and PdSn-based bimetallic catalysts for n-butane dehydrogenation.

Catalysts	n-butane conversion(%)	n-butene yield(%)	Iso-butene yield(%)	n-butene selectivity(%)	Iso-butene selectivity(%)
Pd/Al	6.65	17.25	9.45	63.96	36.04
Pd/AlS	7.65	26.7	17.65	59.93	40.07
PdSn/AlS	56.85	39.3	35.5	53.35	46.65
PdSn/Z	64.35	45.55	42.25	52.56	47.44
PdSn/Sl	68.33	50.65	42.3	51.81	48.19

4. Conclusions

PdSn-based bimetallic catalysts were successfully prepared by cyclic electroless deposition using AlS, Z, and Sl supports. XRD confirmed highly dispersed Pd and Sn species, while TEM showed nanosized metal clusters with improved dispersion after Sn incorporation. EDX verified the successful deposition of Pd and Sn, and BET analysis revealed that the textural properties strongly depended on the support. The PdSn catalysts showed much higher n-butane dehydrogenation activity than monometallic Pd catalysts at 550 °C. The conversion followed the order: PdSn/Sl (68.33%) > PdSn/Z (64.35%) > PdSn/AlS (56.85%) > Pd/AlS (7.65%) > Pd/Al (6.65%). Among all catalysts, PdSn/Sl exhibited the best performance, with the highest n-butane conversion, n-butene yield, and iso-butene yield. The enhanced activity is attributed to Pd–Sn synergistic interaction, improved metal dispersion, and favorable support properties. Overall, PdSn/Sl is a promising catalyst for efficient n-butane dehydrogenation to butenes.

CRediT authorship contribution statement

HKN: Conceptualization, Methodology, Investigation, Formal analysis, Data curation. **PMG**: Conceptualization, Methodology, Investigation, Formal analysis, Data curation, Writing-original draft, Writing - review & editing.

Declaration of Competing Interest

The authors declare that they have no known competing financial interests or personal relationships that could have appeared to influence the work reported in this paper.

Acknowledgments

The authors would like to acknowledge the Department of Chemical Engineering, Central Instruments Facility, and Indian Institute of Technology Guwahati, Assam, India, for providing all the facilities for this work.

References

[1] H.I. Mahdi, O. Muraza, An exciting opportunity for zeolite adsorbent design in separation of C4 olefins through adsorptive separation, Sep. Purif. Technol. 221 (2019) 126–151. https://doi.org/https://doi.org/10.1016/j.seppur.2018.12.004.

[2] M. Gao, G. Zhang, L. Zhao, J. Gao, C. Xu, Research Progress of Basic Catalyst Used in Catalytic Cracking for Olefin Production and Heavy Oil Utilization, Ind. Eng. Chem. Res. 62 (2023) 1215–1226. https://doi.org/10.1021/acs.iecr.2c03939.

[3] R. Saxena, M. De, Enhanced performance of supported Pd-Pt bimetallic catalysts prepared by modified electroless deposition for butane dehydrogenation, Appl. Catal. A Gen. 610 (2021) 117933. https://doi.org/10.1016/j.apcata.2020.117933.

[4] P. Natarajan, H. Abbas, S. Yoon, K. Jung, One-pot synthesis of Pt – Sn bimetallic mesoporous alumina catalysts with worm-like pore structure for n-butane dehydrogenation, J. Ind. Eng. Chem. 63 (2018) 380–390. https://doi.org/10.1016/j.jiec.2018.02.038.

[5] F. Regali, L.F. Liotta, A.M. Venezia, V. Montes, M. Boutonnet, S. Järås, Effect of metal loading on activity, selectivity and deactivation behavior of Pd/silica–alumina catalysts in the hydroconversion of n-hexadecane, Catal. Today 223 (2014) 87–96. https://doi.org/10.1016/j.cattod.2013.08.028.

[6] S.A. Bocanegra, S.R. de Miguel, I. Borbath, J.L. Margitfalvi, O.A. Scelza, Behavior of bimetallic PtSn/Al2O3 catalysts prepared by controlled surface reactions in the selective dehydrogenation of butane, J. Mol. Catal. A Chem. 301 (2009) 52–60. https://doi.org/10.1016/j.molcata.2008.11.006.

[7] B.P. Ajayi, B.R. Jermy, K.E. Ogunronbi, B.A. Abussaud, n-Butane dehydrogenation over mono and bimetallic MCM-41 catalysts under oxygen free atmosphere, Catal. Today 204 (2013) 189–196. https://doi.org/10.1016/j.cattod.2012.07.013.

[8] X. Li, B. Yan, S. Yao, S. Kattel, J.G. Chen, T. Wang, Oxidative dehydrogenation and dry reforming of n -butane with CO 2 over NiFe bimetallic catalysts, Appl. Catal. B Environ. 231 (2018) 213–223. https://doi.org/10.1016/j.apcatb.2018.02.063.

[9] S. Furukawa, M. Endo, T. Komatsu, Bifunctional Catalytic System Effective for Oxidative Dehydrogenation of 1-Butene and n -Butane Using Pd-Based Intermetallic Compounds, ACS Catal. 4 (2014) 3533–3542. https://doi.org/10.1021/cs500920p.

[10] L. Rodríguez, D. Romero, D. Rodríguez, J. Sánchez, F. Domínguez, G. Arteaga, Dehydrogenation of n-butane over Pd–Ga/Al2O3 catalysts, Appl. Catal. A Gen. 373 (2010) 66–70. https://doi.org/10.1016/j.apcata.2009.10.040.

[11] S. Veldurthi, C. Shin, O. Joo, K. Jung, Promotional effects of Cu on Pt / Al 2 O 3 and Pd / Al 2

O 3 catalysts during n-butane dehydrogenation, Catal. Today 185 (2012) 88–93. https://doi.org/10.1016/j.cattod.2011.11.021.

[12] L. Rodríguez, D. Romero, D. Rodríguez, J. Sánchez, F. Domínguez, G. Arteaga, Dehydrogenation of n-butane over Pd-Ga/Al2O3 catalysts, Appl. Catal. A Gen. 373 (2010) 66–70. https://doi.org/10.1016/j.apcata.2009.10.040.

[13] R. Saxena, M. De, Ni/Cu/Ag promoted Pd/Al2O3 catalysts prepared by electroless co-deposition for enhanced butane dehydrogenation, Mater. Chem. Phys. 261 (2021) 124236. https://doi.org/10.1016/j.matchemphys.2021.124236.

[14] D.M. Alonso, S.G. Wettstein, J.A. Dumesic, Bimetallic catalysts for upgrading of biomass to fuels and chemicals, Chem. Soc. Rev. 41 (2012) 8075–8098. https://doi.org/10.1039/c2cs35188a.

[15] M. Sankar, N. Dimitratos, P.J. Miedziak, P.P. Wells, C.J. Kiely, G.J. Hutchings, Designing bimetallic catalysts for a green and sustainable future, Chem. Soc. Rev. 41 (2012) 8099–8139. https://doi.org/10.1039/c2cs35296f.

[16] Z. Wei, J. Sun, Y. Li, A.K. Datye, Y. Wang, Bimetallic catalysts for hydrogen generation, Chem. Soc. Rev. 41 (2012) 7994–8008. https://doi.org/10.1039/c2cs35201j.

[17] L. Deng, H. Miura, T. Shishido, Z. Wang, S. Hosokawa, Elucidating strong metal-support interactions in Pt – Sn / SiO 2 catalyst and its consequences for dehydrogenation of lower alkanes, J. Catal. 365 (2018) 277–291. https://doi.org/10.1016/j.jcat.2018.06.028.

[18] Z. Nawaz, S. Qing, G. Jixian, X. Tang, F. Wei, Effect of Si/Al ratio on performance of Pt–Sn-based catalyst supported on ZSM-5 zeolite for n-butane conversion to light olefins, J. Ind. Eng. Chem. 16 (2010) 57–62. https://doi.org/10.1016/j.jiec.2010.01.021.

[19] P.M. Gawal, A.K. Golder, Green Synthesis of Z-Scheme SnO_2/CdS Heterostructures: Density Functional Theory Calculation and Photocatalytic CO_2 Reduction to Methanol and Hydrogen,

Langmuir (2026). https://doi.org/10.1021/acs.langmuir.5c05827.

[20] P.M. Gawal, J. Ishrat, K. Bhattacharyya, A.K. Golder, Experimental and Theoretical Studies on Photocatalytic CO_2 Reduction to HCOOH by Biomass-Derived Carbon Dots Embedded Phytochemical-Based CdS Quantum Dots, Langmuir 41 (2025) 11161–11172. https://doi.org/10.1021/acs.langmuir.5c01002.

[21] P.M. Gawal, A.K. Golder, Novel ternary Z-scheme nanocomposites: Biomass-derived carbon dots decorated on g-C3N4(Thiourea) -g-C3N4(Urea) heterostructures for photocatalytic CO2 reduction to CO and H2, Int. J. Hydrogen Energy 199 (2026) 152856. https://doi.org/10.1016/j.ijhydene.2025.152856.

464

Supplementary Files

This is a list of supplementary files associated with this preprint. Click to download.

- SupplemntoryInformation.docx